

# **Long-wavelength 640 x 486 GaAs/AlGaAs Quantum Well Infrared Photodetector Snap-shot Camera**

**Sarath D. Gunapala, Sumith V. Bandara, John K. Liu, Winn Hong,  
Mani Sundaram, Paul D. Maker, Richard E. Muller, Craig A. Shott,  
Ron Carralejo,**

## **ABSTRACT**

A 9  $\mu\text{m}$  cutoff 640 x 486 snap-shot quantum well infrared photodetector (QWIP) camera has been demonstrated. The performance of this QWIP camera is reported including indoor and outdoor imaging. The noise equivalent differential temperature ( $\text{NE} \cdot T$ ) of 36 mK has been achieved at 300 K background with f/2 optics. This is in good agreement with expected focal plane array sensitivity due to the practical limitations on charge handling capacity of the multiplexer, read noise, bias voltage and operating temperature.

This was jointly sponsored by the Jet Propulsion Laboratory Director's Research and Development Fund, the Ballistic Missile Defense Organization / Innovative Science & Technology Office, and the National Aeronautics and Space Administration, Office of Space Science.

Sarath D. Gunapala, Sumith V. Bandara, John K. Liu, Winn Hong, Mani Sundaram, Paul D. Maker, Richard E. Muller are with Center for Space Microelectronics Technology, Jet Propulsion Laboratory, California Institute of Technology, Pasadena, CA 91109.

Craig A. Shott, Ron Carralejo, with Amber, A Raytheon Company, Goleta, CA 93117.

## I INTRODUCTION

In recent years, quantum well infrared photodetectors (QWIPs) have shown very good imaging performance at high-background conditions using large area 128 x 128 and 256 x 256 highly uniform focal plane arrays (FPAs). These FPAs are fabricated entirely from large bandgap materials which are easy to grow and process. It is now possible to obtain large uniform FPAs of QWIPs tuned to detect light at wavelengths from 6 to 25  $\mu\text{m}$  in the GaAs/ $\text{Al}_x\text{Ga}_{1-x}\text{As}$  material system [1-4]. Currently, there is a tremendous interest in long-wavelength QWIPs due to infrared (IR) imaging systems that require large format long-wavelength infrared (LWIR) FPAs for myriad applications, including night vision, navigation, flight control, early warning systems, Earth observing systems, astronomy, etc. Improvements in QWIP performance depends largely on the minimization of the parasitic current that plagues all light detectors, the dark current (the current that flows through a biased detector in the dark, i.e., with no photons impingement on it) and improving the quantum efficiency. As we have discussed previously [1,5,6], at temperatures above 45 K, the dark current of the QWIPs having cutoff wavelengths in the 8-12  $\mu\text{m}$  spectral region are entirely dominated by classic thermionic emission of ground state electrons into the energy continuum. Therefore, minimizing this dark current component is critical to the commercial success of the QWIP as it allows the highly-desirable 60-70 K operating temperature which can be easily achieved by single stage Stirling coolers.

In order to reduce this parasitic dark current, we have designed the bound-to-quasibound quantum well by placing the first excited state exactly at the well top. The previous QWIPs were called bound-to-continuum, because the first excited state was a continuum energy band above the well top (typically 10 meV). Dropping the first excited state to the well top increases the barrier to thermionic emission (roughly the energy height from the ground state to the well top) by ~10-15 meV in our bound-to-quasibound QWIP than in the bound-to-continuum device structure, causing the dark

current to drop by a factor of  $\sim 6$  at a temperature of 70 K (5-6). The dark current-voltage curve of the 8.3  $\mu\text{m}$  peaked bound-to-quasibound QWIP is shown in Figure 1. This compares well with the factor of  $\sim 6$  drop we have expected from the theoretical estimations.

## II. TEST STRUCTURE RESULTS

A single period of the multi-quantum well (MQW) structure consists of a 45 Å well of GaAs (doped  $n \sim 5 \times 10^{17} \text{ cm}^{-3}$ ) and a 500 Å barrier of  $\text{Al}_{0.3}\text{Ga}_{0.7}\text{As}$ . Stacking identical quantum wells (typically 50) together increases photon absorption. Ground state electrons are provided in the detector by doping the GaAs well layers with Si. This photosensitive MQW structure is sandwiched between 0.5  $\mu\text{m}$  GaAs top and bottom contact layers doped  $n = 5 \times 10^{17} \text{ cm}^{-3}$ , grown on a semi-insulating GaAs substrate by molecular beam epitaxy (MBE). Then a 1.0  $\mu\text{m}$  thick GaAs cap layer on top of a 300 Å  $\text{Al}_{0.3}\text{Ga}_{0.7}\text{As}$  stop-etch layer was grown *in situ* on top of the device structure to fabricate the light coupling 2-D grating pattern. The MBE grown QWIP structure was processed into 200  $\mu\text{m}$  diameter mesa test structures (area =  $3.14 \times 10^{-4} \text{ cm}^2$ ) using wet chemical etching, and Au/Ge ohmic contacts were evaporated onto the top and bottom contact layers.

The detectors were back illuminated through a 45° polished facet [5] and a responsivity spectrum is shown in Figure 2. The responsivity of the detector peaks at 8.3  $\mu\text{m}$  and the peak responsivity ( $R_p$ ) of the detector is 150 mA/W at bias  $V_B = -2 \text{ V}$ . The spectral width and the cutoff wavelength are  $\Delta\lambda/\lambda = 10\%$  and  $\lambda_C = 8.8 \mu\text{m}$  respectively. The bias dependent peak responsivity of the detector was measured and it is small up to about  $V_B = -0.5 \text{ V}$ . Beyond that it increases nearly linearly with bias reaching  $R_p = 395 \text{ mA/W}$  at  $V_B = -5 \text{ V}$ . This behavior of responsivity versus bias is typical for a bound-to-quasibound QWIP. The peak quantum efficiency was 17.5% at bias  $V_B = -3 \text{ V}$  for a 45° double pass. The lower quantum efficiency is due to the lower well doping density ( $5 \times 10^{17} \text{ cm}^{-3}$ ) as it is necessary to suppress the dark current at the highest possible

operating temperature. A peak quantum efficiency as high as 25% has already been achieved with typical well doping densities (i.e.,  $\sim 1 \times 10^{18} \text{ cm}^{-3}$ ). Due to lower readout multiplexer well depth (i.e.,  $9 \times 10^6$  electrons), a lower dark current is mandatory to achieve a higher operating temperature. In this case, the highest operating temperature of 70 K was determined by the cooling capacity of the liquid nitrogen laboratory dewar. The operating temperature of 70 K has been achieved by pumping on liquid nitrogen.

The photoconductive gain  $g$  was experimentally determined using [5]  $g = i_n^2 / 4eI_D B + 1/2N$ , where  $B$  is the measurement bandwidth,  $N$  is the number of quantum wells, and  $i_n$  is the current noise, which was measured using a spectrum analyzer. The photoconductive gain of the detector was 0.2 at bias  $V_B = -3 \text{ V}$  and it reached 0.56 at high bias  $V_B = -5 \text{ V}$ . Since the gain of QWIP is inversely proportional to the number of quantum wells  $N$ , the better comparison would be the well capture probability  $p_c$ , which is directly related to the gain [5] by  $g = 1/Np_c$ . The calculated well capture probabilities are 25% at low bias (i.e.,  $V_B = -1 \text{ V}$ ) and 3.5% at high bias (i.e.,  $V_B = -5 \text{ V}$ ) which together indicate the excellent hot-electron transport in this device structure. The peak detectivity is defined as  $D_p^* = R_p \sqrt{AB} / i_n$ , where  $R_p$  is the peak responsivity,  $A$  is the area of the detector and  $A = 3.14 \times 10^{-4} \text{ cm}^2$ . The measured peak detectivity at bias  $V_B = -3.0 \text{ V}$  and temperature  $T = 70 \text{ K}$  is  $2.2 \times 10^{11} \text{ cm} \cdot \text{Hz/W}$ . Figure 3 shows the bias dependence of peak detectivity at temperatures 70 and 77 K. These detectors show background limited performance (BLIP) at bias  $V_B = -3 \text{ V}$  and temperature  $T = 72 \text{ K}$  for 300 K background with  $f/2$  optics.

### III. QWIP IMAGING FOCAL PLANE ARRAYS

Very long-wavelength QWIPs with random reflectors have shown relatively high quantum efficiencies with large test device structures. It is not possible to achieve the similar high quantum efficiencies with random reflectors on small focal plane array pixels due to the reduced width-to-height aspect ratios. In addition, it is difficult to fabricate

random reflectors for shorter wavelength detectors than for very long-wavelength detectors (i.e., 15  $\mu\text{m}$ ) due to the fact that feature sizes of random reflectors are linearly proportional to the peak wavelength of the detectors. For example, the minimum feature size of the random reflectors of 15  $\mu\text{m}$  cutoff and 9  $\mu\text{m}$  cutoff FPAs were 1.25 and 0.6  $\mu\text{m}$  respectively and it is difficult to fabricate sub-micron features by contact photolithography. As a result, the random reflectors of the 9  $\mu\text{m}$  cutoff FPA were less sharp and had fewer scattering centers compared to the random reflectors of the 15  $\mu\text{m}$  cutoff QWIP FPA. As discussed before [5,8], more IR light can be coupled to the QWIP detector structure by incorporating a two dimensional (2-D) periodic grating surface on top of the detectors which also removes the light coupling limitations and makes two dimensional QWIP imaging arrays feasible. This two dimensional grating structure was fabricated on the detectors by using standard photolithography and  $\text{CCl}_2\text{F}_2$  selective dry etching.

After the 2-D grating array (calculations of the 2-D grating parameters and light coupling experiments were extensively discussed in references 8 and 9) was defined by the photolithography and dry etching, the photoconductive QWIPs of the 640 x 486 FPAs were fabricated by wet chemical etching through the photosensitive  $\text{GaAs}/\text{Al}_x\text{Ga}_{1-x}\text{As}$  multi-quantum well layers into the 0.5  $\mu\text{m}$  thick doped GaAs bottom contact layer. The pitch of the FPA is 25  $\mu\text{m}$  and the actual pixel size is 18 x 18  $\mu\text{m}^2$ . The cross gratings on top of the detectors were then covered with Au/Ge and Au for Ohmic contact and reflection. Figure 4 shows twelve processed QWIP FPAs on a 3 inch GaAs wafer. Indium bumps were then evaporated on top of the detectors for Si readout circuit (ROC) hybridization. A single QWIP FPA was chosen and hybridized (via indium bump-bonding process) to a 640 x 486 direct injection silicon readout multiplexer (Amber AE-181) and biased at  $V_B = -2.0$  V. Figure 5 shows a size comparison of this large area long-wavelength QWIP FPA to a quarter. At temperatures below 70 K, the signal-to-noise-ratio of the system is limited by multiplexer readout noise, and shot-noise of the photo current. At temperatures above 70 K, temporal noise due to the QWIP's

higher dark current becomes the limitation. As mentioned earlier this higher dark current is due to thermionic emission and thus causes the charge storage capacitors of the readout circuitry to saturate. Since the QWIP is a high impedance device, it should yield a very high charge injection coupling efficiency into the integration capacitor of the multiplexer. In fact Bethea *et al.* (2) have demonstrated charge injection efficiencies approaching 90%. Charge injection efficiency can be obtained from (3)

$$\eta_{inj} = \frac{g_m R_{Det}}{1 + g_m R_{Det}} \left[ \frac{1}{1 + \frac{j\omega C_{Det} R_{Det}}{1 + g_m R_{Det}}} \right] \quad (1)$$

where  $g_m$  is the transconductance of the MOSFET and is given by  $g_m = eI_{Det}/kT$ . The differential resistance  $R_{Det}$  of the pixels at -2 V bias is  $5.4 \times 10^{10}$  Ohms at  $T = 70$  K and detector capacitance  $C_{Det}$  is  $1.4 \times 10^{-14}$  F. The detector dark current  $I_{Det} = 24$  pA under the same operating conditions. According to equation (1) the charge injection efficiency  $\eta_{inj} = 99.5\%$  at a frame rate of 30 Hz. The FPA was back-illuminated through the flat thinned substrate membrane (thickness  $\approx 1300$  Å). This thinned GaAs FPA membrane has completely eliminated the thermal mismatch between the silicon CMOS readout multiplexer and the GaAs based QWIP FPA. Basically, the thinned GaAs based QWIP FPA membrane adapts to the thermal expansion and contraction coefficients of the silicon readout multiplexer. Thus, thinning has played an extremely important role in the fabrication of large area FPA hybrids. In addition, this thinning has completely eliminated the pixel-to-pixel optical cross-talk of the FPA. This initial array gave very good images with 99.97% of the pixels working, demonstrating the high yield of GaAs technology. The operability was defined as the percentage of pixels having noise equivalent differential temperature less than 100 mK at 300 K background with f/2 optics and in this case operability happens to be equal to the pixel yield.

We have used the following equation to calculate the noise equivalent temperature difference (NE $\cdot$  T) of the FPA.

where  $D_B^*$  is the detectivity,  $NE\Delta T = \frac{\sqrt{AB}}{D_B^* (dP_B / dT) \sin^2(\theta / 2)}$  is the blackbody derivative of the integrated blackbody power with respect to temperature, and  $\theta$  is the field of view angle [i.e.,  $\sin^2(\theta/2) = (4f^2 + 1)^{-1}$ , where  $f$  is the f number of the optical system]. The background temperature  $T_B = 300$  K, the area of the pixel  $A = (18 \mu\text{m})^2$ , the f number of the optical system is 2, and the frame rate is 30 Hz. Figure 6 shows the experimentally measured  $NE \bullet T$  histogram of the FPA at an operating temperature of  $T = 70$  K, bias  $V_B = -2$  V at 300 K background with  $f/2$  optics and the mean value is 36 mK. This agrees reasonably well with our estimated value of 25 mK based on test structure data. The read noise of the multiplexer is 500 electrons. The 44% shortfall of  $NE \bullet T$  is mostly attributed to unoptimized detector bias (i.e.,  $V_B = -2$  V was used instead of optimum  $V_B = -3$  V based on detectivity data as a function of bias voltage as shown in Fig. 3), decrease in bias voltage across the detectors during charge accumulation (common in many direct injection type readout multiplexers) and read noise of the readout multiplexer. The experimentally measured peak quantum efficiency of the FPA was 2.3% (lower focal plane array quantum efficiency is attributed to 51% fill factor and 30% reflection loss from the GaAs back surface). Therefore, the corrected quantum efficiency of a focal plane detectors is 6.5% and this corresponds to an average of two pass of IR radiation (equivalent to a single 45° pass) through the photosensitive multi-quantum well region.

#### IV FOCAL PLANE ARRAY CAMERA

A 640 x 486 QWIP FPA hybrid was mounted onto a 84-pin lead-less chip carrier and installed into a laboratory dewar which is cooled by liquid nitrogen to demonstrate a LWIR imaging camera (shown in Figure 7). The FPA was cooled to 70K by pumping on liquid nitrogen and the temperature was stabilized by regulating the pressure of gaseous nitrogen. The other element of the camera is a 100 mm focal length AR coated germanium lens, which gives a  $9.2^\circ \times 6.9^\circ$  field of view. It is designed to be transparent in the 8-12  $\mu\text{m}$  wavelength range to be compatible with the QWIP's 8-9  $\mu\text{m}$  operation. A commercially available Amber ProView<sup>TM</sup> image processing system was used to obtain clock signals for readout multiplexer and to perform digital data acquisition and non-uniformity corrections. The resolution of digital data acquisition of the camera is 12-bits, which determines the instantaneous dynamic range of the camera (i.e., 4096), however, the dynamic range of QWIP is 85 Decibels.

The measured mean NE $\cdot$  T of the QWIP camera is 36 mK at an operating temperature of  $T = 70$  K and bias  $V_B = -2$  V at 300 K background with f/2 optics. This is in good agreement with expected focal plane array sensitivity due to the practical limitations on charge handling capacity of the multiplexer, read noise, bias voltage and operating temperature. The uncorrected NE $\cdot$  T non-uniformity (which includes a 1% non-uniformity of the ROC and a 1.4% non-uniformity due to the cold-stop in front of the FPA not yielding the same field of view to all the pixels) of the 311,040 pixels of the 640 x 486 FPA is about 5.6% (= sigma/ mean). Figure 8 shows the noise histogram of this first unoptimized 640 x 486 QWIP FPA and the higher sigma/mean was due to the reduced number of samples acquired during the measurement. The non-uniformity after two-point (17 $^\circ$  and 27 $^\circ$  Celsius) correction improves to an impressive 0.04%. As mentioned earlier, this high yield is due to the excellent GaAs growth uniformity and the mature GaAs processing technology. After two point correction, measurements of the residual nonuniformity were made at temperatures ranging from 10 $^\circ$  C (the cold



temperature limit of the blackbody source) up to 40° C. The non-uniformity at each temperature was found by averaging 16 frames, calculating the standard deviation of the pixel-to-pixel variation of the 16 frame average and then dividing by the mean output, producing non-uniformity that may be reported as a percentage. For camera systems that have NE• T of about 30 mK, the corrected image must have less than 0.1% non-uniformity in order to be standard television (TV) quality. Only at temperature of 38 Celsius the camera's residual non-uniformity has exceeded the 0.1% non-uniformity threshold. Figure 8 shows residual non-uniformity plotted versus scene temperature. The 33 Celsius window where the correction is below 0.1% is based on the measured data and one extrapolated data point at 5 Celsius.

Video images were taken at a frame rate of 30 Hz at temperatures as high as  $T = 70$  K using a ROC capacitor having a charge capacity of  $9 \times 10^6$  electrons (the maximum number of photoelectrons and dark electrons that can be counted in the integration time of each detector pixel). Figure 9 (a) and (b) show two frames of video image taken with this long-wavelength 640 x 486 QWIP camera. The image in Figure 9(a) was taken in the night (around midnight) and it clearly shows where automobiles were parked during the day time. Figure 9(b) show blades of a fast turning chopper wheel. The sharp straight edges of the chopper wheel demonstrate the snap-shot mode of operation. These high resolution images comparable to standard TV, demonstrate the high operability (i.e., 99.9%) and the stability (i.e., lower residual uniformity and 1/f noise) of the 640 x 486 long-wavelength QWIP staring array camera .

It should be noted that these initial unoptimized FPA results are far from optimum. The light coupling gratings were not optimized (as described earlier) for maximum light coupling efficiency, no anti-reflection coatings were used on the backside of the FPA, and finally the multiplexer used was not optimized to supply the proper bias required by photoconductive QWIPs (i.e., AE-181 was optimized for photovoltaic InSb FPAs). Implementation of these improvements should significantly enhance the QWIP FPA operating temperature (i.e., 77 K for 9  $\mu$ m).

## **ACKNOWLEDGMENTS**

The research described in this paper was performed by the Center for Space Microelectronics Technology, Jet Propulsion Laboratory, California Institute of Technology.

## FIGURE CAPTIONS

Fig. 1 Dark current-voltage curves of 8.3  $\mu\text{m}$  peaked bound-to-quasibound at temperatures from  $T = 40\text{-}100\text{ K}$ . Data were taken with a 200  $\mu\text{m}$  diameter test structure and normalized to  $18 \times 18\ \mu\text{m}^2$  pixel.  $T = 70\text{K}$  normalized dark currents were compared with experimentally obtained dark currents at several bias voltages between  $V_B = -1\text{V}$  and  $V_B = -3\text{V}$ , and those agreed with in  $\pm 5\%$ .

Fig. 2 Responsivity spectrum of a bound-to-quasibound LWIR QWIP test structure at temperature  $T = 77\text{ K}$ . The spectral response peak is at 8.3  $\mu\text{m}$  and the long wavelength cutoff is at 8.8  $\mu\text{m}$ .

Fig. 3 Detectivity as a function of bias voltage at temperatures  $T = 70$  and  $77\text{K}$ .

Fig. 4 Twelve 640 x 486 QWIP focal plane arrays on a 3 in. GaAs wafer.

Fig. 5 A size comparison of the 640 x 486 long-wavelength QWIP FPA to a quarter.

Fig. 6 Noise equivalent temperature difference ( $\text{NE} \cdot T$ ) histogram of the 311,040 pixels of the 640 x 486 array showing a high uniformity of the FPA. The uncorrected non-uniformity ( $= \text{standard deviation/mean}$ ) of this unoptimized FPA is only 5.6% including 1% non-uniformity of ROC and 1.4% non-uniformity due to the cold-stop not being able to give the same field of view to all the pixels in the FPA.

Fig. 7 Picture of the 640 x 486 long-wavelengths QWIP camera.

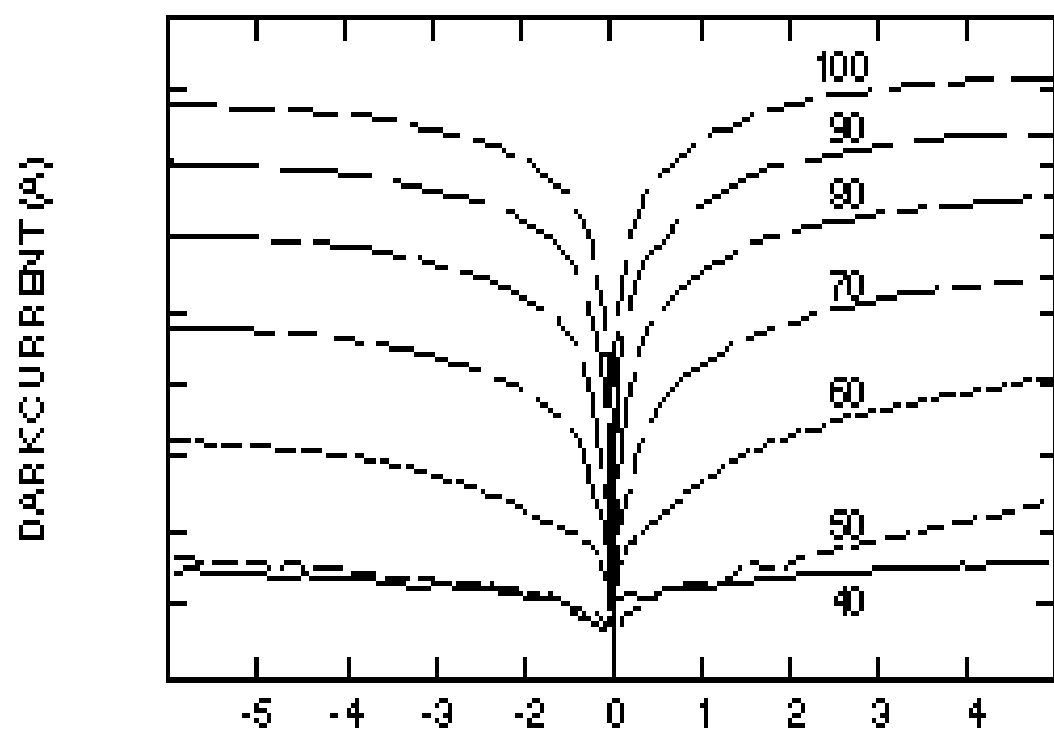
Fig. 8 Residual nonuniformity after two point correction as a function of scene temperature. This corrected uniformity range is comparable to 3-5  $\mu\text{m}$  IR cameras.

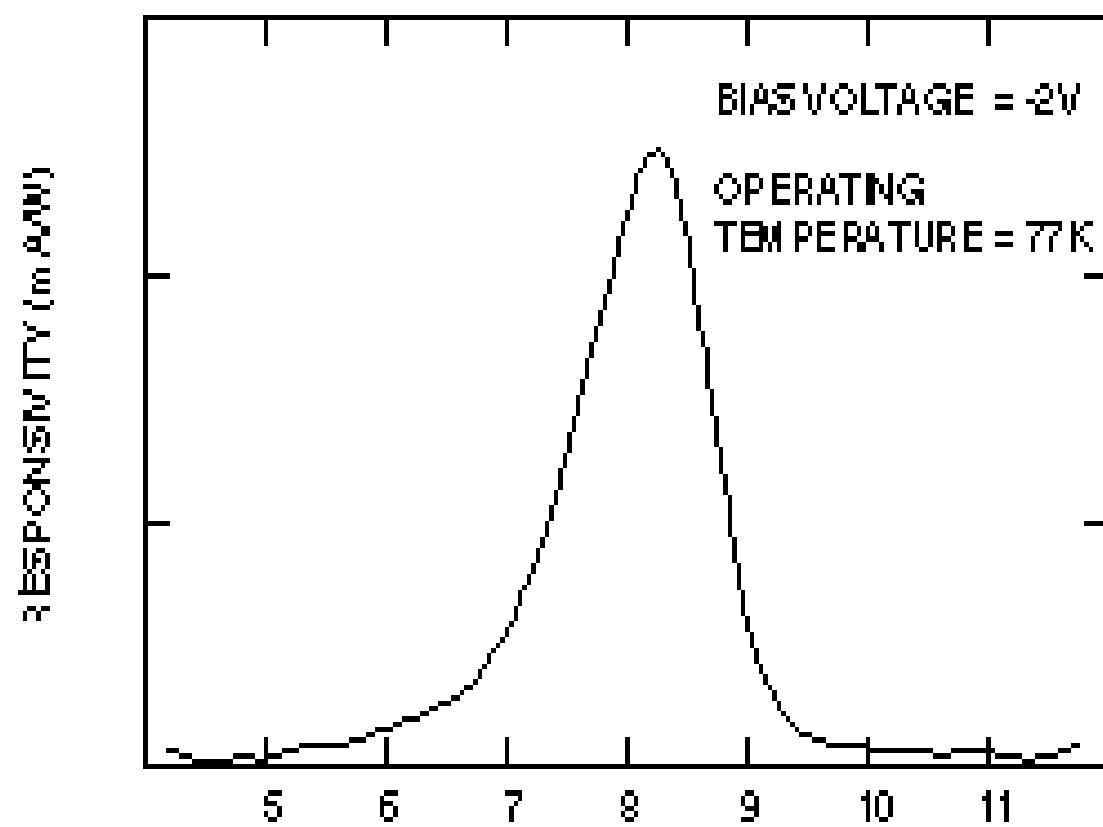
Fig. 9 (a) this picture was taken in the night (around midnight) and it clearly shows where automobiles were parked during the day time. This image demonstrates the high sensitivity of the 640 x 486 long-wavelength QWIP staring array camera. Figure (b) show blades of a fast turning chopper wheel. The sharp straight edges of the chopper wheel demonstrate the snap-shot mode of operation.

## REFERENCES

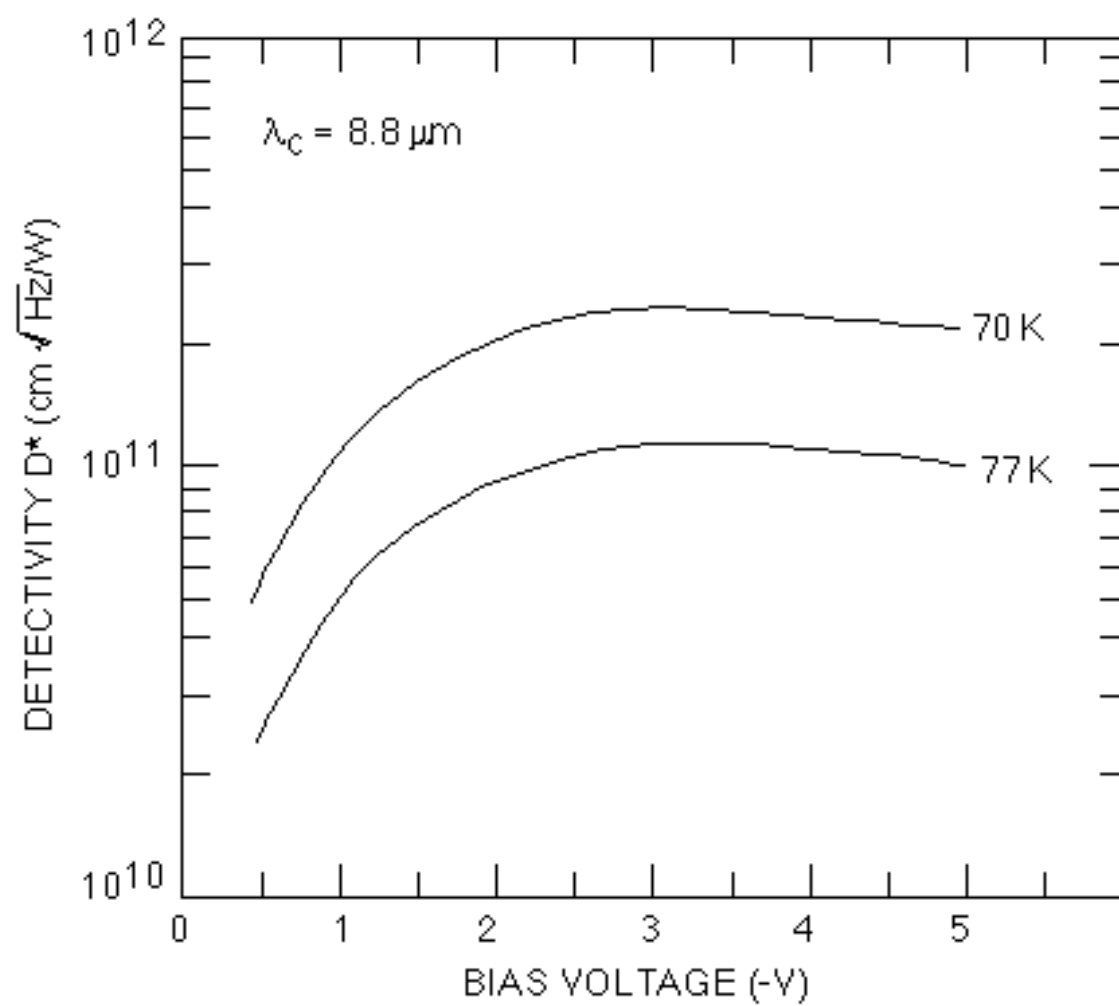
1. Sarath D. Gunapala, John K. Liu, Jin S. Park, Mani Sundaram, Craig A. Shott, Ted Hoelter, True-Lon Lin, S. T. Massie, Paul D. Maker, Richard E. Muller, and Gabby Sarusi" 9  $\mu\text{m}$  Cutoff 256 x 256 GaAs/Al<sub>x</sub>Ga<sub>1-x</sub>As Quantum Well Infrared Photodetector Hand-Held Camera", *IEEE Trans. Electron Devices*, **44**, pp. 51-57, 1997.
2. C. G. Bethea, B. F. Levine, M. T. Asom, R. E. Leibenguth, J. W. Stayt, K. G. Glogovsky, R. A. Morgan, J. D. Blackwell, and W. J. Parrish, "Long Wavelength Infrared 128 x 128 Al<sub>x</sub>Ga<sub>1-x</sub>As/GaAs Quantum Well Infrared Camera and Imaging System," *IEEE Trans. Electron. Devices*, vol. 40, pp. 1957-1963, 1993.
3. L. J. Kozlowski, G. M. Williams, G. J. Sullivan, C. W. Farley, R. J. Andersson, J. Chen, D. T. Cheung, W. E. Tennant, and R. E. DeWames, "LWIR 128 x 128 GaAs/AlGaAs Multiple Quantum Well Hybrid Focal Plane Array," *IEEE Trans. Electron. Devices* , vol. ED-38, pp. 1124-1130, 1991.
4. W. A. Beck, T. S. Faska, J. W. Little, J. Albritton, and M. Sensiper, *Proceedings of the Second International Symposium on 2-20  $\mu\text{m}$  Wavelength Infrared Detectors and Arrays: Physics and Applications*, October 10-12, 1994, Miami Beach, Florida.
5. S. D. Gunapala and K. M. S. V. Bandara, *Physics of Thin Films*, Academic Press, **21**, 113 (1995).
6. Sarath D. Gunapala, Jin S. Park, Gabby Sarusi, True-Lon. Lin, John K. Liu, Paul D. Maker, Richard E. Muller, Craig A. Shott, and Ted Hoelter, "15  $\mu\text{m}$  128 x 128 GaAs/AlGaAs Quantum Well Infrared Photodetector Focal Plane Array Camera", *IEEE Trans. Electron Devices*, **44**, pp. 45-50, 1997.

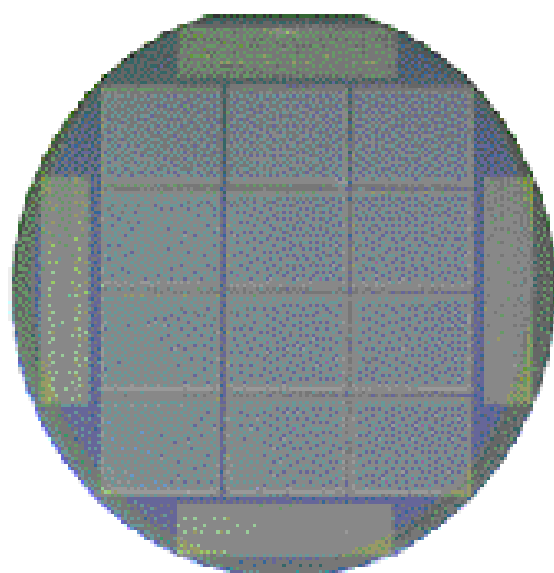
7. G. Sarusi, B. F. Levine, S. J. Pearton, K. M. S. V. Bandara, and R. E. Leibenguth, "Improved performance of quantum well infrared photodetectors using random scattering optical coupling," *Appl. Phys. Lett.*, vol. 64, pp. 960-962, 1994.
8. Sumith Bandara, Sarath Gunapala, John Liu, Winn Hong and Jin Park, "Optical coupling mechanisms in quantum well infrared photodetectors", *Photodetectors; Materials and Devices*, G. Brown and M. Razeghi, editor, Proc. SPIE **2999** (1997).
9. J. Y. Andersson and L. Landqvist, "Grating-coupled quantum-well infrared detectors: Theory and performance", *J. Appl. Phys.* **71**, pp.3600-3610, 1992.

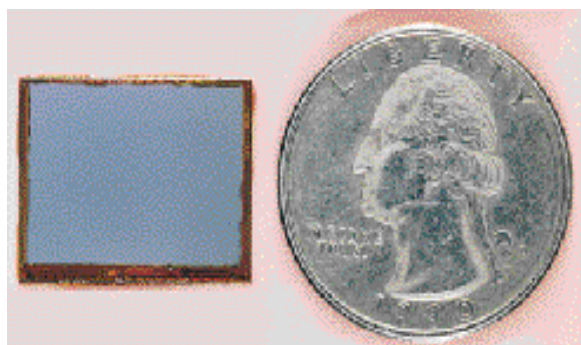




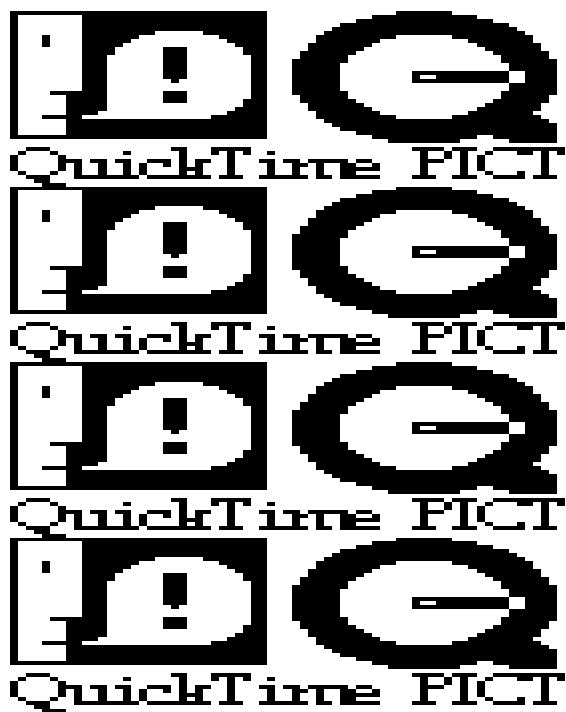


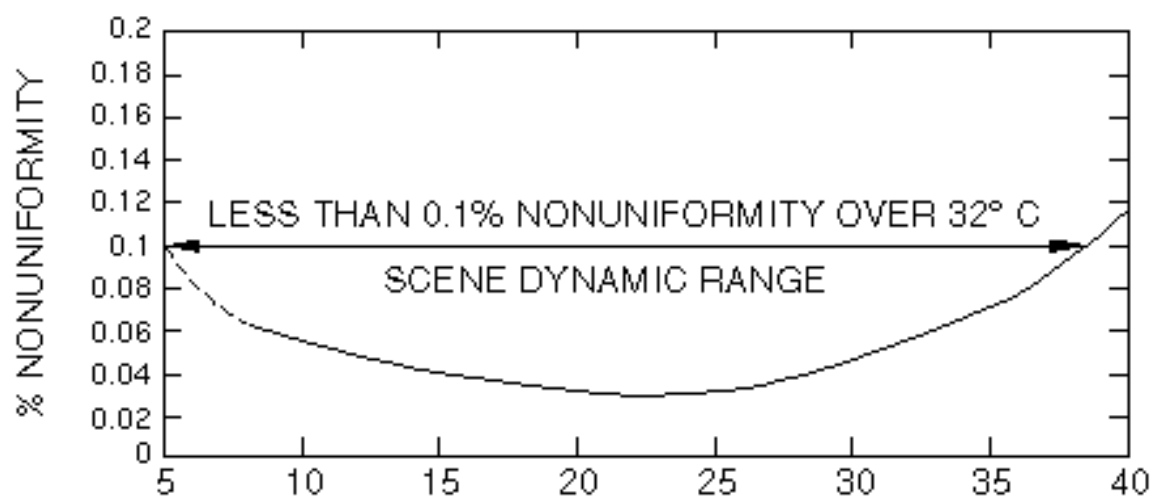












(a)



(b)

